

**7th International Meeting
on
Wind Turbine Noise
Rotterdam 2-5 May 2017**

**High Fidelity Airfoil Trailing Edge Noise Predictions via
Lattice-Boltzmann Simulations**

F. Manegar **University of Siegen, 57068 Siegen, Germany**
E-Mail: **farhan.manegar@uni-siegen.de**

T. Carolus **University of Siegen , 57068 Siegen, Germany**
E-Mail: **thomas.carolus@uni-siegen.de**

S. Erbslöh **Senvion SE, 24783 Osterröfeld, Germany**
E-Mail: **sascha.erbsloeh@senvion.com**

ABSTRACT

Sound emissions from an isolated airfoil immersed in a free-stream are caused by a number of mechanisms. In some installations such as wind turbines, the turbulent boundary layer interacting with the trailing edge (TE) is, in most instances, dominant. Objective of this study is the validation of numerical simulations with experimentally obtained measurements of TE noise from a Somers S834 airfoil section. Measurements were conducted in the University of Siegen acoustic wind tunnel. The numerical method chosen is the Lattice-Boltzmann scheme as it promises a significant reduction in CPU time compared to Navier-Stokes based LES simulation. Two different setups are investigated. The first setup ("2D") is an airfoil section with only a relatively short span-wise extension (7.5% of chord length). Installation effects due to the wind tunnel are not taken into account. In the second setup ("3D"), the computational domain covers the wind tunnel and the entire semi-anechoic room. At first the 2D configuration is analyzed. Compared to experiments the predicted boundary layer induced surface pressure, near-field velocity fluctuations close to the TE and far field sound pressure are in good agreement. Predictions for the configuration "3D" show fair agreement with the direct recording of far field sound pressure spectra, but not with near field pressure and velocity fluctuations. Lastly the results of the 2D configuration are compared with the results of a Navier-Stokes based LES simulation, whose data is available from a previous study of the same setup.

1. INTRODUCTION

The ongoing energy revolution requires installing wind turbines in the vicinity of residential areas, at least in areas with dense population. Wind turbines are known to produce noise, which may be a reason for annoyance. Hence there arises an ongoing effort to reduce wind turbines further. Since half a century numerous studies have been conducted to understand the mechanism by which a flow encountering airfoil emits noise. One early study is by BROOKS et al [1] of a NACA 0012 airfoil section. They identified five airfoil self-noise mechanisms due to boundary layer phenomena. Noise from a full scale wind turbine was analyzed e.g. by OERLEMANS et al [2] employing an experimental and semi-analytical method. They showed that the blade trailing edge (TE) region contributes the most to the overall wind turbine noise. TE noise is caused due to the scattering of the turbulent boundary layer at the TE of an airfoil. A recent study was conducted by GERHARD [3-5] on TE noise and on active/passive ways to reduce it. In this study, the computational aero-acoustic (CAA) method "CURLE's analogy [6] based on a numerical large eddy simulations (LES)" was utilized.

In general CAA methods are of two types: Direct and hybrid. In an hybrid method, an acoustic

analogy is required to predict the far field noise. By contrast, in a direct method, the far field acoustics and the near field flow variables is simulated simultaneously. The usage of the Lattice BOLTZMANN Method (LBM) as a direct tool to predict far field noise has been successfully demonstrated by several studies [7, 8]. LBM has also been used to simulate a section of an airfoil, using both direct and hybrid methods, especially to investigate TE noise [9, 10]. The objective of this study is to use LBM to simulate the TE noise from a Somers S834 airfoil, validate it with the experimental results and draw a comparison with LES/CURLE results from GERHARD's study.

2. Governing Equations

LBM is different from the traditional Computational Fluid Dynamics (CFD) methods. Traditional CFD methods solve partial differential NAVIER-STOKES (N-S) equations, to simulate the fluid. On the other hand, LBM uses discrete BOLTZMANN equations to simulate the flow at kinetic level [11]. Particle distribution functions (PDF), which are defined as the number density of molecules at position x and speed v at a time t , are used by BOLTZMANN equations to capture the kinetic behavior of particles in the lattice world. The basic difference between traditional CFD and LBM lies in this fact, that the LBM approach has much simpler physics to deal with, compared to solving the non-linear PDEs in the N-S approach. LBM is inherently time-dependent. Fluid properties like density and velocity are derived from these PDFs. Such a discretization strategy leads to conservation of mass, momentum and energy. The discrete Lattice BOLTZMANN equations and the associated terms with it are

$$f_i(x + c_i \Delta t, t + \Delta t) - f_i(x, t) = C_i(x, t), \quad (1)$$

where f_i denotes the movement of the distribution of particles in the i -th direction. $c_i \Delta t$ and Δt are the space and time increments.

The right hand side of the eq. (1) consists of the collision term and is called as BHATNAGAR GROSS and KROOK [12] collision operation. Its main function was found out to be that it drives the velocity distribution function towards its equilibrium distribution. The collision term

$$C_i(x, t) = -\frac{\Delta t}{\tau} [f_i(x, t) - f_i^{eq}(x, t)]. \quad (2)$$

consists of relaxation time τ which describes how quickly the velocity distribution function relaxes towards equilibrium and it relates to the fluid viscosity. It uses a 3D cubic lattice D3Q19 to discretize the velocity space into 19 discrete speeds. The usage of D3Q19 enables enough number of velocity components for sufficient lattice symmetry to recover the N-S equations [13]. The f_i^{eq} term is the equilibrium distribution function and in order to recover macroscopic hydrodynamics [14], f_i^{eq} has been chosen in such a way that the conservation laws are satisfied. As mentioned earlier, the fluid properties like density and velocity are obtained by taking the moment summations over the velocity vectors:

$$\rho(x, t) = \sum_i f_i(x, t), \quad \rho u(x, t) = \sum_i c_i f_i(x, t) \quad (3)$$

In order to recover the compressible N-S equations, CHAPMAN-ENSKOG expansion can be used for small Mach number (Ma). The resulting equation of state obeys the ideal gas law: $p = \rho RT$. The relaxation time parameter τ is related to the kinematic viscosity of the fluid as

$$\tau = \frac{\nu}{RT} + \frac{\Delta t}{2}. \quad (4)$$

[15].

In this study, a turbulence model called very large-eddy simulation (VLES) is used. It consists of a two-equation k - ε renormalization group (RNG) [16]. These two equations are further modified to incorporate a swirl correction factor [17]. This enables the resolution of unsteady large-scale vortices in regions, where these can be resolved.

In high Reynolds number (Re) applications, a wall function is used to model the effect of the boundary layer on the rest of the flow because fully resolving the near wall region is computationally expensive. Hence the cell closest to a surface is assumed to obey the law of the wall. A hybrid wall function smoothly transitions from a turbulent wall function (i.e. a logarithmic profile) at high y^+ values to a viscous wall function (i.e. a linear profile) at low y^+ values as given in eq. (5). Along with the velocity profiles, this hybrid wall function is coupled with a wall model pressure gradient

extension to account for the effects of favorable and adverse pressure gradient (APG) on the near-wall boundary layer profile [18].

$$u^+ = u(y)/u_T = \begin{cases} y^+ & \text{for } y^+ < 5, \\ g(y^+) & \text{for } 5 < y^+ < 35, \\ \frac{1}{k} \log(y^+) + C_1 & \text{for } y^+ > 35. \end{cases} \quad (5)$$

In this study, the commercial software Exa PowerFLOW™ 5.0c has been used to set up two different types of simulation case in order to simulate the TE noise emitted.

3. SIMULATION CASE SETUP

The case investigated here is a SOMERS S834 airfoil segment, which has a chord based Re of $3.5 \cdot 10^5$ with tripping bands positioned at 17% and 76% of chord length on the suction and pressure side such that it mimics a Re of $3.5 \cdot 10^6$. It has a chord length $c = 0.2$ m and an aspect ratio of 1.33. The inlet velocity, $U_{ref} = 25.55$ m/s and the effective angle of attack (AOA) is 4.7° . Since the airfoil is placed in a jet flow, a correction factor is applied to the angle of attack as suggested by BROOKS et al [19]. This leads to a geometrical AOA of 12.7° . It has to be noted that the previous study comprising of the LES simulations and experimental measurement also considered this correction factor while calculating the AOA .

The first case setup is called $2D$, where only a segment of the span (7.5% chord) is simulated with periodic boundary condition in the span. By simulating only a segment of the span, the advantage lies in the fact that a very fine layer of cells can be used in the near wall region of the airfoil and is still computationally affordable. This leads to surface y^+ of less than 5 on the airfoil segment and hence a wall model is not used. However, a direct acoustic prediction is only possible with a correction factor as introduced by OBERAI [10] for reduced span and cyclic boundary conditions.

As already mentioned, LBM has an advantage compared to traditional CFD approaches, that it can solve the full compressible flow equations for determining both the hydrodynamic and acoustic pressure fluctuations. Hence, in order to utilize this advantage of LBM, a second simulation case called $3D$ is set up. In this setup, the entire anechoic room, where the acoustic measurements were held, is simulated. The simulation domain of both setups are shown in Fig. 1. Obviously, with such a large

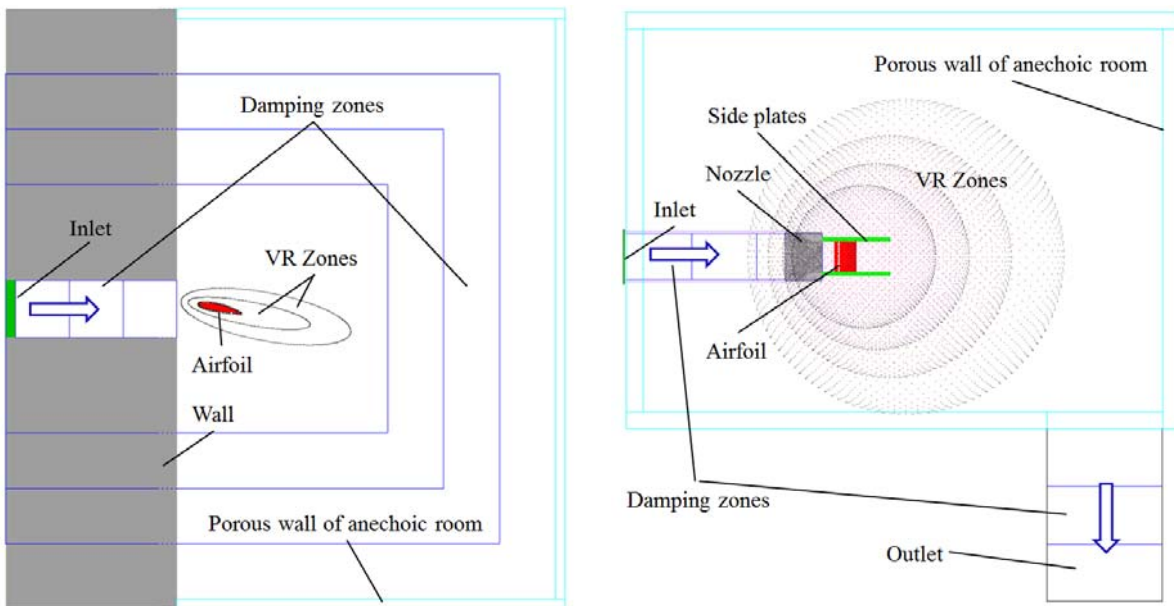


Fig. 1 Left: Simulation domain (top view) of $2D$ setup; right: Simulation domain (side view) of $3D$ setup.

computational domain, the near wall cells can not be as fine as they are in the $2D$ setup. They are four times coarser than the $2D$ setup. Another advantage of such a configuration is that the installation

effects (side plates) are also considered.

In LBM, discretization takes place using a strategy called variable resolution (VR) zones. Each VR zone consists of cubical volume cells called voxels. The size of voxels increase by the factor two in adjacent VR zones. In Fig. 2, the various VR zones for the 3D setup are shown.

In both setups, a velocity is provided at the inlet boundary condition and the outlet boundary condition is set as atmospheric pressure. The inlet and outlet region are modeled as damping zones to avoid acoustic reflections. The simulated Ma ($Ma = 0.075$) is chosen the same as in experiment, such that the acoustic waves propagate at the same speed as they do in experiment.

Before getting into the results section, there are two interesting aspects to be checked; the wall model that would be used and the percentage of resolved turbulence. The surface y^+ is depicted in Fig. 3. It is observed that due to finer resolution near the wall, 2D setup has y^+ value less than 5 in most portions of the airfoil surface. This means that the velocity profile would be calculated and a wall model would not be used. Due to coarser mesh, the 3D setup has surface y^+ considerably greater than 5 in most of the airfoil surface, except for some regions near TE on the suction side (SS). In Fig. 3, only a section of airfoil span in the 3D setup is shown, whereas the entire span is shown in the 2D setup.

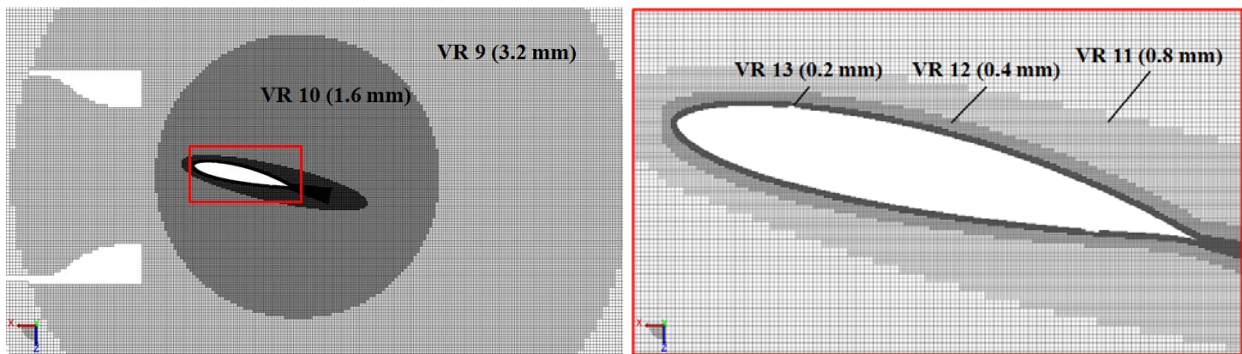


Fig. 2 Left: Top view of VR zones (plane cut at mid span) in the 3D setup; right: Zoomed view of the same.

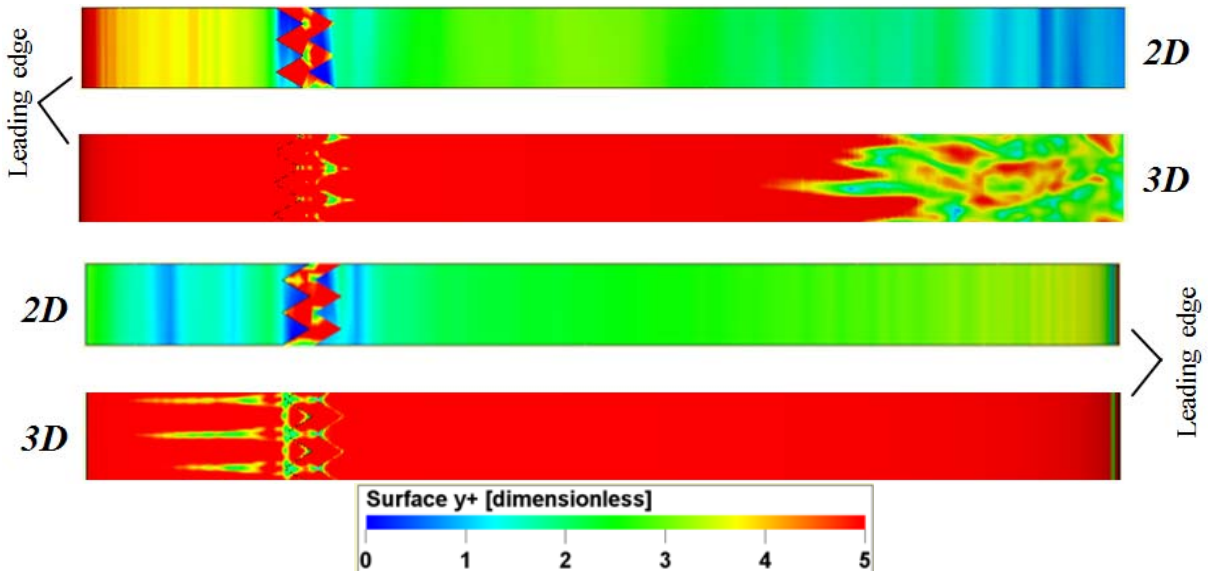


Fig. 3 Top: Surface y^+ on the suction side; bottom: Surface y^+ on the pressure side.

Exa PowerACOUSTICS™ (one of the post processing tools in PowerFLOW™) allows the access to information on the REYNOLD's stresses or fluctuation kinetic energy (FKE) and the total turbulence kinetic energy (TTKE). In order to compute the amount of resolved turbulence, a percentage of FKE over TTKE is taken and shown in Fig. 4. It is noticed that after the trip, 2D setup has more amount of turbulence resolved than the 3D setup on both sides of the airfoil. Table 1 summarizes other interesting information regarding the setups.

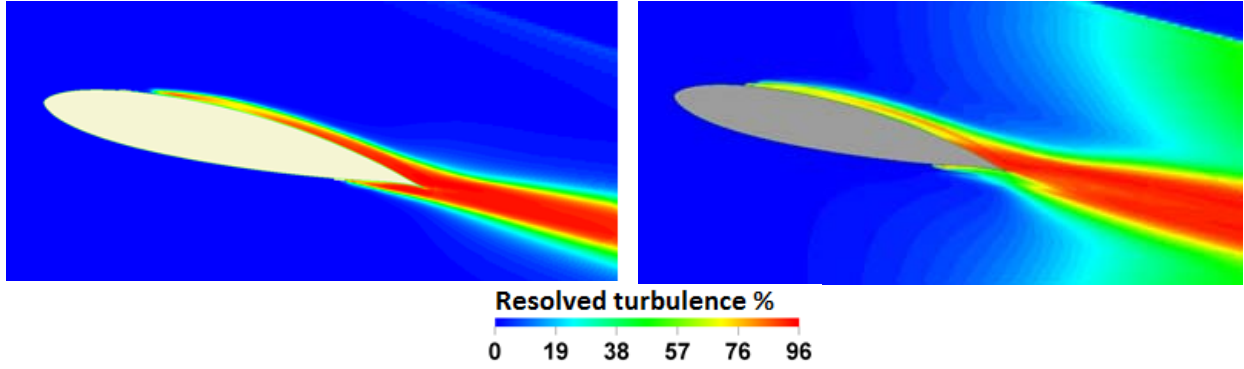


Fig. 4 Left: Resolved turbulence % - plane cut at mid span: 2D setup; right: 3D setup.

Table 1 Details of simulation setups in LBM

Parameter	2D	3D
Time step at finest voxel VR zone	$3.3 \cdot 10^{-7}$ s	$2.66 \cdot 10^{-7}$ s
Finest voxel	0.0586 mm	0.2 mm
Total no. of voxels	28 mio	129 mio
CPU hours (for 0.5 s physical time)	37000	25000

4. FLOW FIELD RESULTS

All results shown here are taken after the flow field had reached a statistically steady state. Unless otherwise stated, all the unsteady quantities in LBM are captured with a sampling frequency $f_s = 20$ kHz for 36 through-flow times $T_f = c/U_{ref}$. The power spectral density (PSD) shown in the spectral analysis is obtained using the *pwelch* routine in Matlab™ Vers. R2014b ($\Delta f_{ref} = 1$ Hz, $p_0 = 2 \cdot 10^{-5}$ Pa).

The mean pressure distribution in terms of the pressure coefficient $c_p = p_{static}/p_{dynamic}$ on the airfoil surface is shown in Fig. 5. The abscissa is such that $x/c = 0$ corresponds to the leading edge (LE) and $x/c = 1$ to the trailing edge (TE). The values are time averaged for 12 T_f . It is observed that the results from

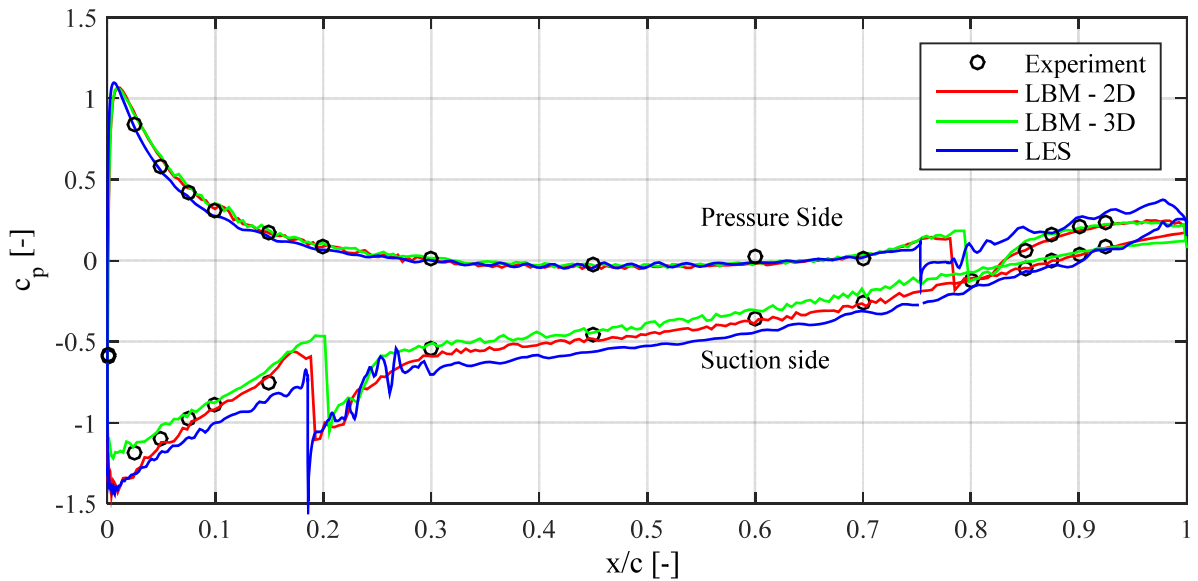


Fig. 5 Mean pressure distribution on the airfoil surface.

both LBM setups as well as LES show a good agreement with the experiment. The sudden jumps in the

pressure distribution on both sides are due to the tripping.

Fig. 6 shows the root-mean-square (RMS) value of fluctuating surface pressure p'_{rms} , normalized with dynamic free stream pressure p_{dyn} near the trailing edge region on the SS. Since such measurement was not done experimentally, only a comparison between LBM and LES is drawn. The LBM surface pressure fluctuations have higher values compared to LES. But in the trailing edge region ($x/c > 0.9$), LBM 2D and LES show the same tendency but not LBM 3D. Experimentally, the blade pressure fluctuations have been recorded at chord wise position $x/c = 0.9$.

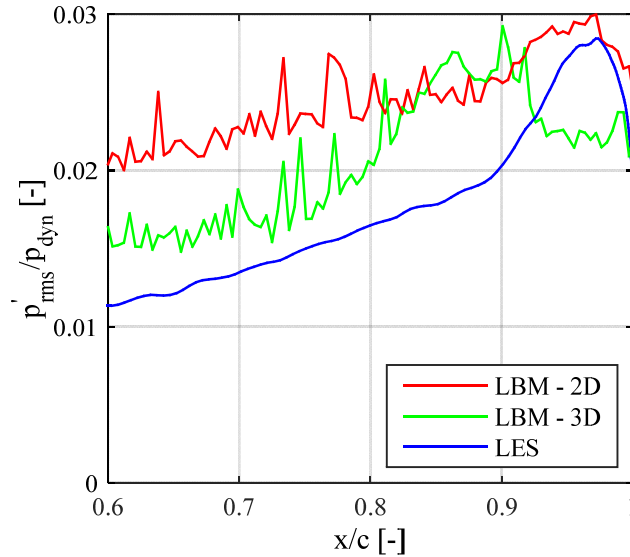


Fig. 6 Simulation predicted pressure fluctuations in the TE region on the SS.

In Fig. 7, the PSD of pressure fluctuations G_{xx} , at this position is compared for all setups. Here the availability of experimental measurement enables us to realize which among the three simulation setups produce similar tendency as experiment and it is apparently the 2D setup which has the same shape as experimental spectrum. But there is an overprediction in all three simulation setups. However, it is observed that the 3D setup produces higher PSD values in the lower frequency range (< 1000 Hz) and less in the higher frequency range. This might be due to the coarser voxels in the 3D setup which were required given the available computational resources.

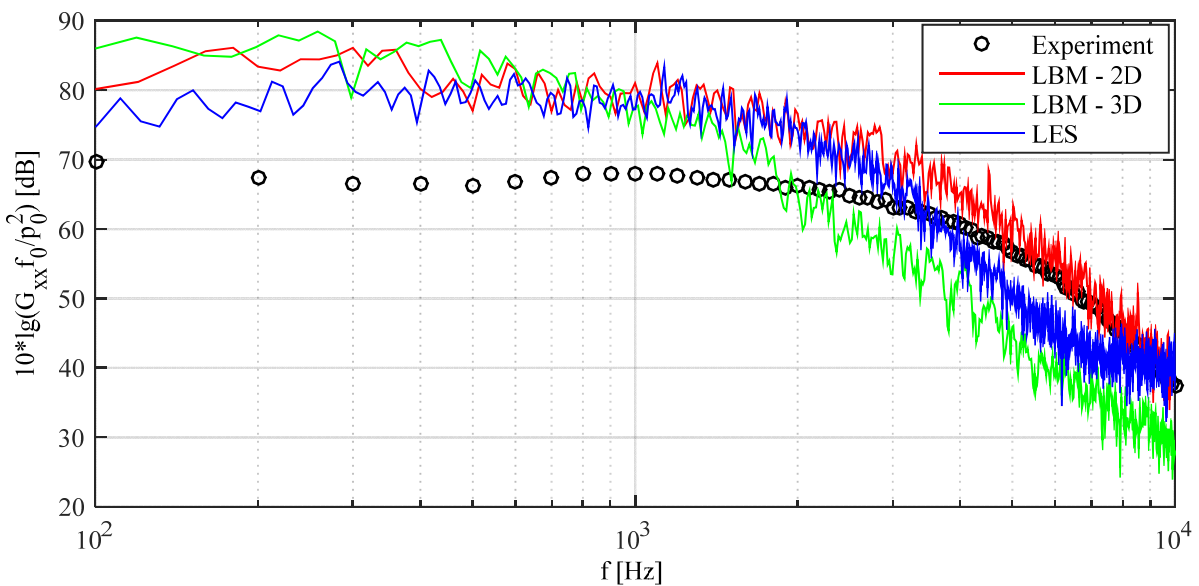


Fig. 7 Experiment and simulation predicted surface pressure spectrum ($x/c = 0.9$ on SS).

The next interesting comparison are boundary layer details on the SS. Fig. 8 shows the comparison

of boundary layer displacement thickness δ^* , normalized with chord for all setups. It is observed that the LBM 3D overpredicts the boundary layer displacement thickness near the trailing edge whereas LBM 2D has a fair agreement with experiment.

In Fig. 9 (upper row) the velocity profiles perpendicular to the surface near the TE on the SS is plotted for three different chord wise positions, $x/c = 0.9, 0.95$ and 1 respectively. Note that y is always perpendicular to wall with $y/c = 0$ at the wall. It is observed that there are some deviations in the velocity profiles compared to experiment in all three simulation setups. Despite the fact that both are LBM simulations (2D and 3D) of the same airfoil, one could observe a clear difference between the velocity profile near the wall. This implies that in 2D setup a wall model is not used, whereas in 3D setup it is used.

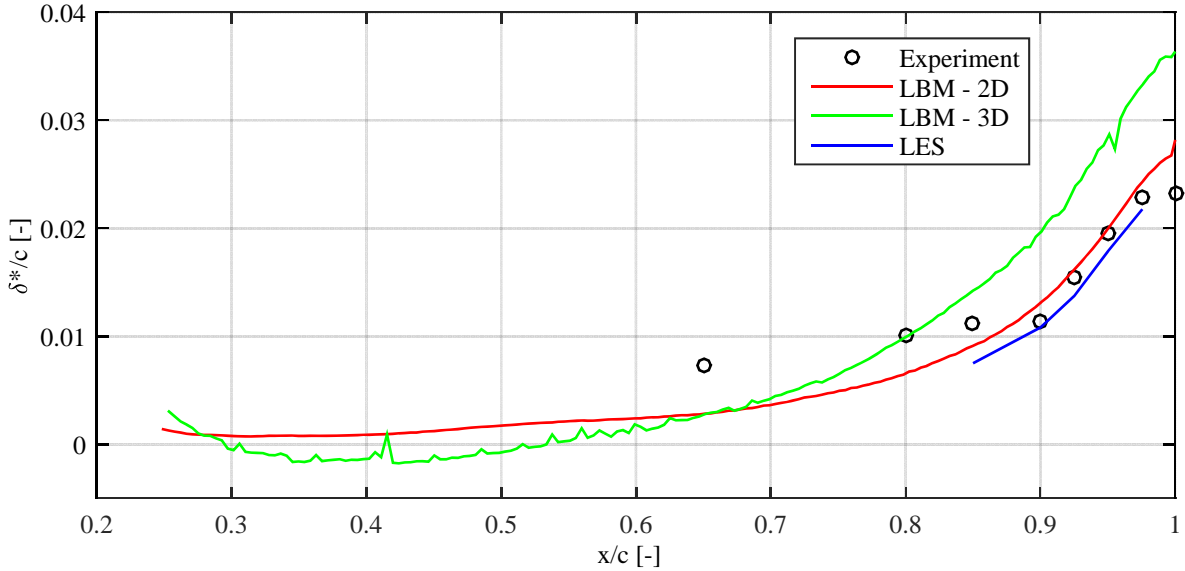


Fig. 8 Boundary layer displacement thickness (SS).

The turbulence intensity

$$TI = u_{rms}' / U_{ref} \quad (6)$$

in the boundary layer is shown in the lower row of Fig. 9 for the same chord wise positions as velocity profiles. In the LBM 2D it matches quite well with the experiment, but LBM 3D overpredicts at all three positions, especially at the TE.

Fig. 10 shows the PSD of velocity fluctuations at a point $y/c = 0.005$ on the SS for two chord wise positions near the TE, $x/c = 0.975$ and 1 respectively. The LBM 2D spectrum shows very good agreement with experiment till 3 kHz and the spectrum falls down after that, owing to the fact that it is modeled and not resolved anymore. And the spectrum of LBM 3D falls down starting from the low frequency range and doesn't match with the experiment. At the TE ($x/c = 1$), LBM 2D matches better with experiment than the LES till 3 kHz.

5. Acoustic Results

As mentioned earlier, LBM is advantageous because the far field pressure fluctuations are measured directly using probes in the simulation domain. In the 3D setup, the microphone probes directly capture the far field pressure fluctuations as it is done in experiment, whereas in the 2D setup, due to reduced span and cyclic boundary conditions, a correction factor has to be added to the direct probe measurements. For low Ma flows, OBERAI [10] recommends a frequency dependent correction factor

$$\beta = 10 \log_{10} \left(\frac{fb^2}{aR} \right), \quad (7)$$

where b is the segmented span, a is the speed of sound and R is the observer distance. This correction factor has been applied to the direct probes measured in the 2D setup. In all setups (experiment and simulations), the microphones were placed at 3 locations: $1.5c$ on either side of airfoil from TE and $1.5c$ on the SS from LE as shown in Fig. 11. All recordings were captured with a $f_s = 52$ kHz. The approach of segmented span in LBM 2D is valid only when the span wise coherence decays within the simulated span. The coherence function

$$\gamma^2(f) = \frac{|G_{ab}(f)|^2}{G_{aa}(f)G_{bb}(f)} \quad (8)$$

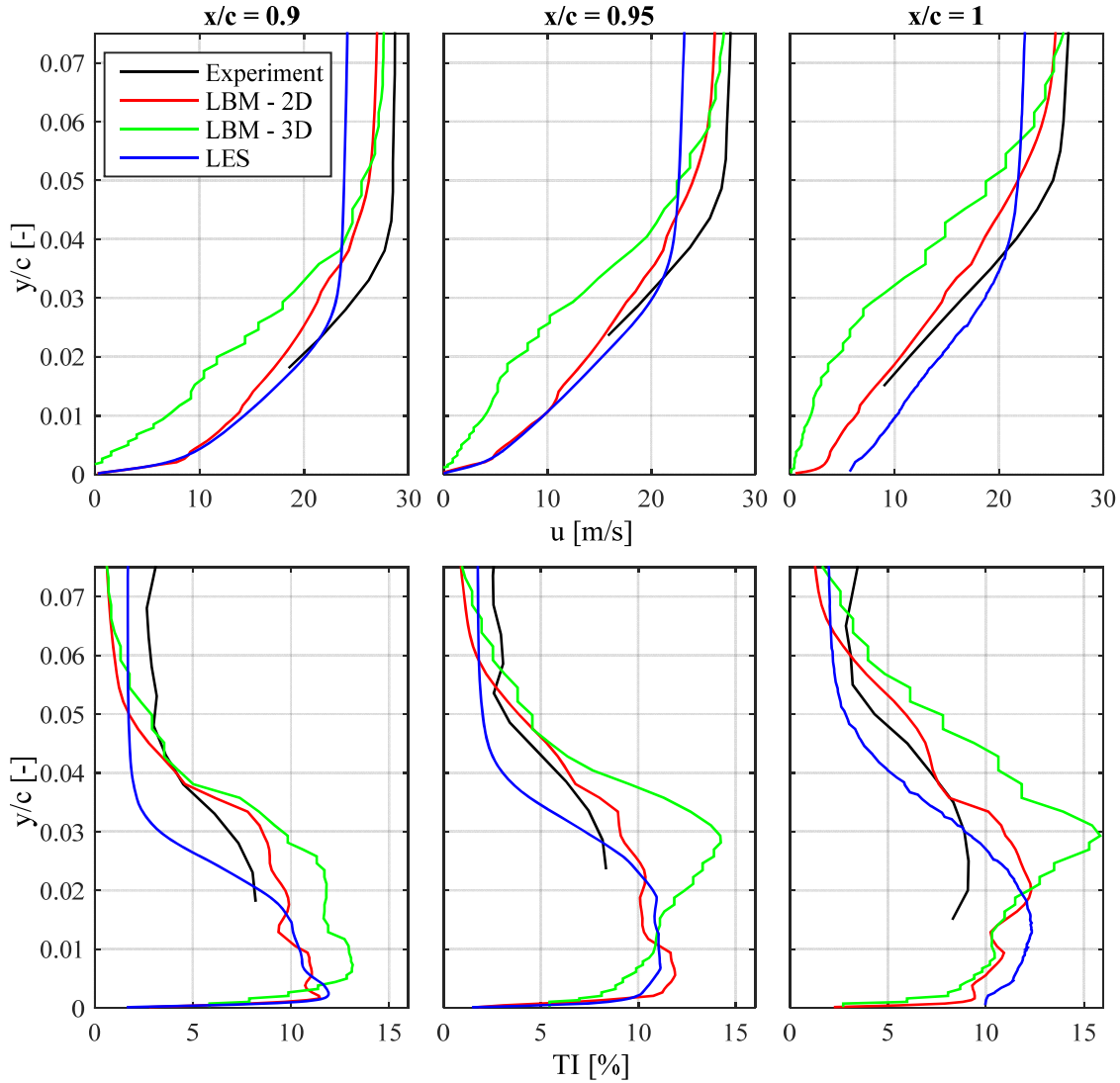


Fig. 9 Top: Velocity distribution; bottom: Turbulence intensity in the turbulent boundary layer on the SS in the TE region.

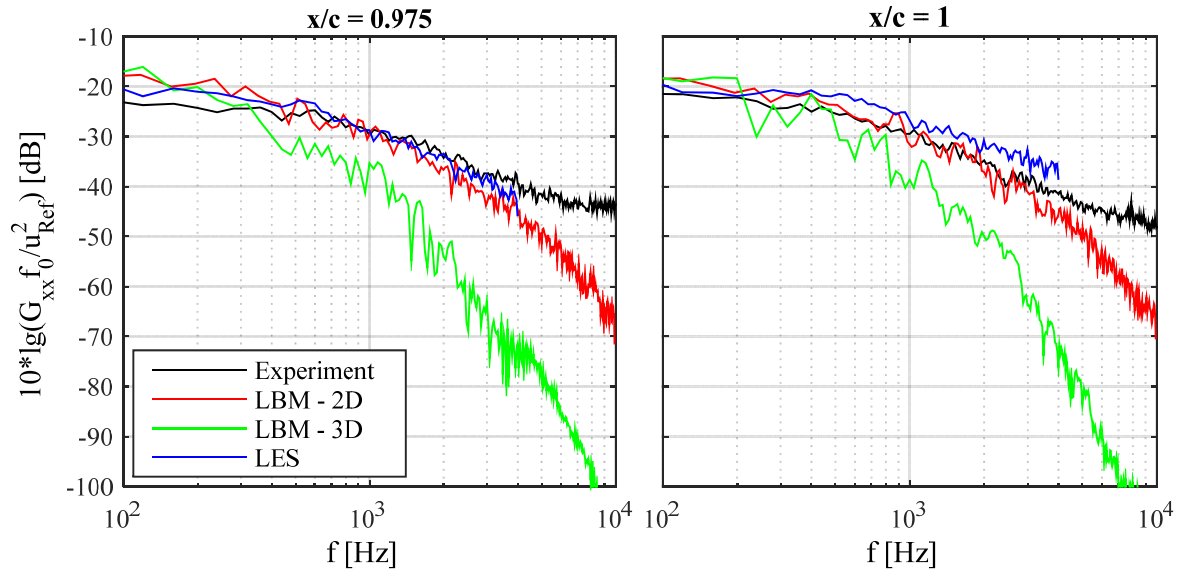


Fig. 10 Experiment and simulation predicted velocity spectrum at $y/c = 0.005$ on the SS.

is a function of the power spectral densities G_{aa} and G_{bb} and the cross power spectral density G_{ab} of signals a and b . In this study it is obtained using the *mscohere* routine in Matlab[®] Vers. R2014b ($\Delta f = 40$ Hz). Span wise coherence is calculated at chord wise position $x/c = 0.95$ on the SS. Fig. 12 shows the contour plot of span wise coherence of the 2D setup. The y-axis covers the simulation domain in spanwise direction (z is the distance in span). Only the frequency range between 300 Hz - 2000 Hz has been plotted, since it falls in the interest of TE noise evaluation. It is observed that for frequencies less than 500 Hz, a complete decay of span wise coherence is not observed. Extending the simulation domain in the spanwise direction will capture the largest flow structures correctly. However, the very strong coherent structures (with coherence function > 0.4) decay well in the frequency range less than 500 Hz.

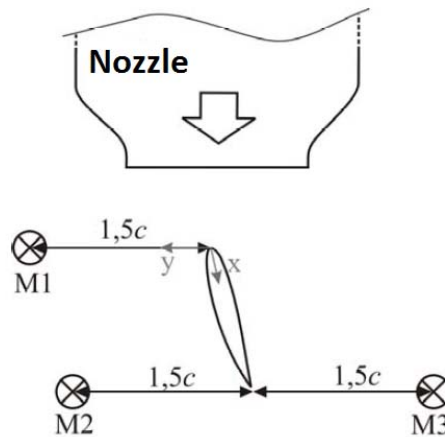


Fig. 11 Schematic diagram of microphone locations.

Fig. 13 depict key results of this study: the spectral sound pressure level (SPL) (average of 3 microphones according to Fig. 11). The signal-to-background noise ratio is large enough only in the frequency range of 300 Hz to 2000 Hz, where the TE noise can be identified in the experiment. As stated by GERHARD [4], the acoustic evaluations in his study of the same setup showed that the airfoil TE noise is the most prominent noise source from frequencies of 160 Hz to 3000 Hz and that one can expect a hump dominating the TE noise spectrum to lie in a frequency range between 350 Hz and 550 Hz. It is observed that the LBM 2D and experimental measurement match quite well in the frequencies

ranging from 400 Hz to 1000 Hz. It is also observed that the direct *SPL* predicted by LBM 3D is overpredicted in the TE noise region. This again correlates with the results seen earlier in blade pressure fluctuations spectrum due to coarser cells.

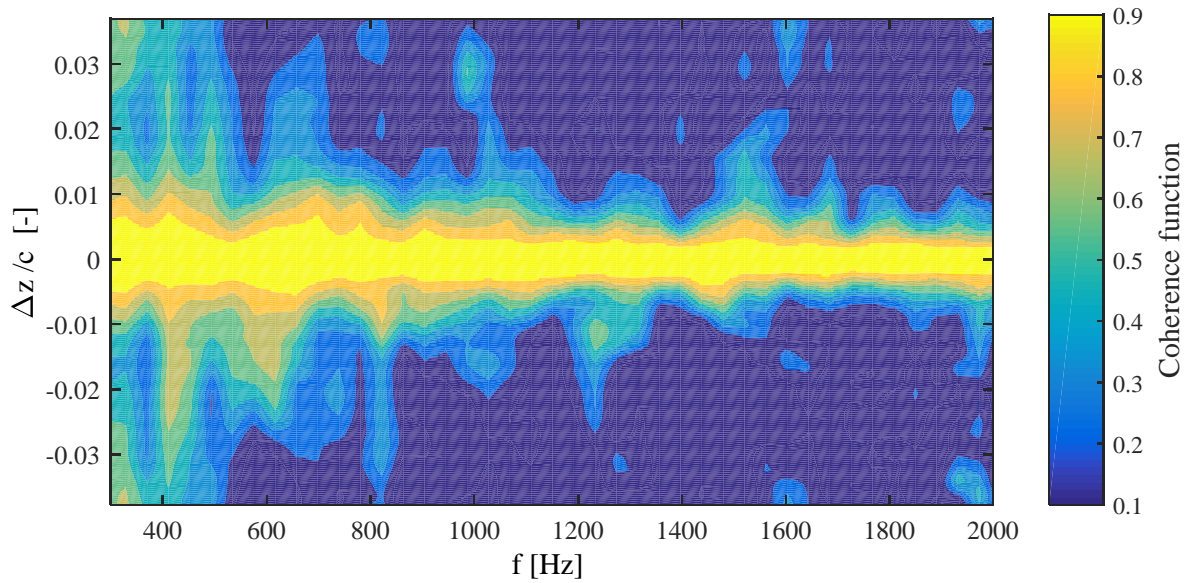


Fig. 12 Span wise coherence of blade pressure for LBM 2D at $x/c = 0.95$ on the SS.

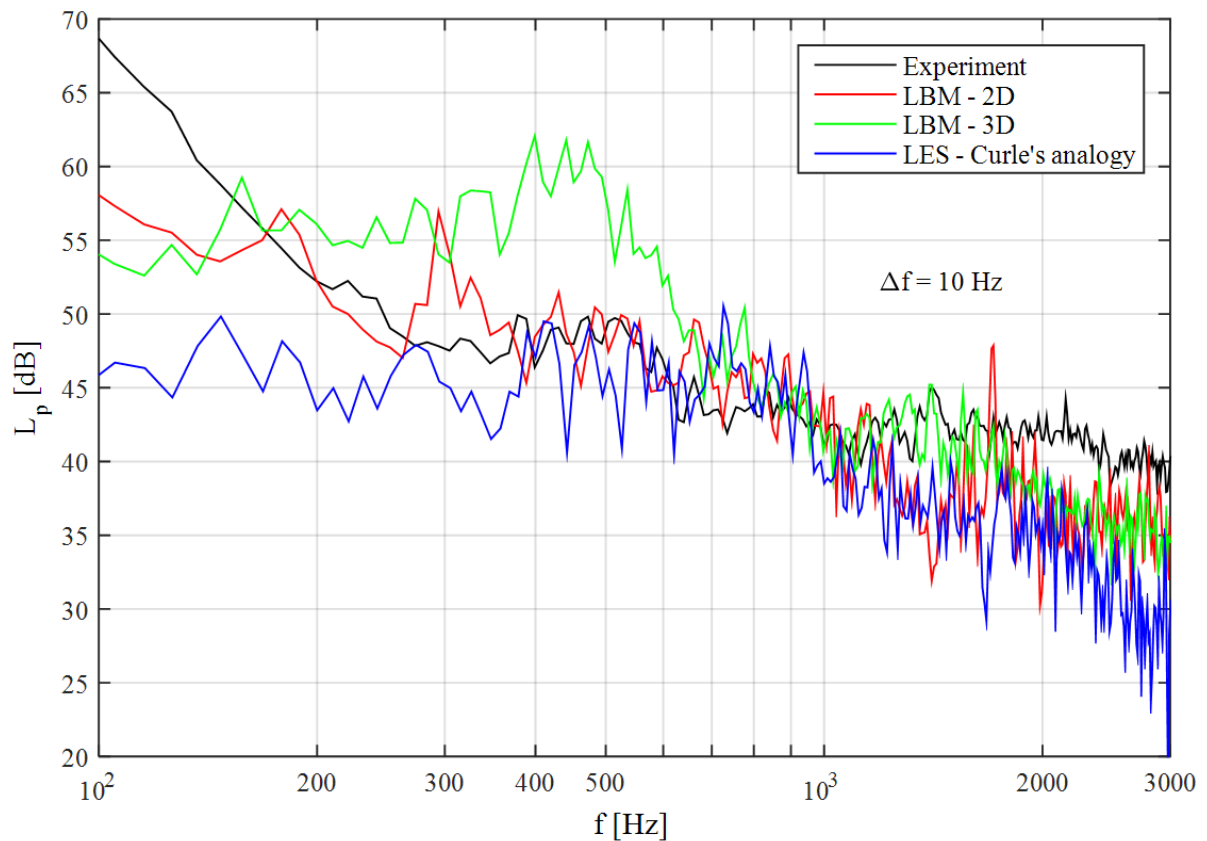


Fig. 13 SPL at observer points according to Fig. 11 (all microphones averaged).

Fig. 14 shows the instantaneous dilatation $\frac{1}{\rho} \frac{\partial \rho}{\partial t}$ field in LBM 2D setup. It is confirmed that the

major acoustic source is identified at the TE, where the acoustic waves propagate from the TE region due to diffraction of turbulent eddies on the TE.

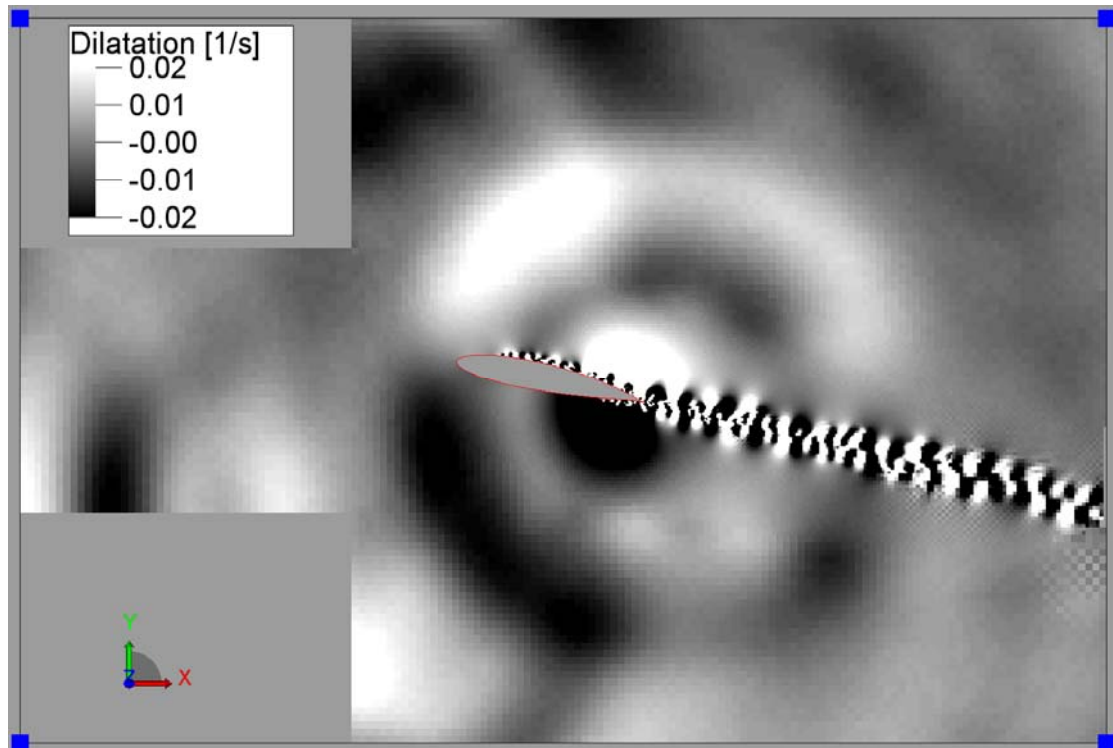


Fig. 14 Instantaneous image of dilatation field in LBM 2D (plane cut at mid span).

6. Conclusion

Aero-acoustic simulation of a S834 airfoil section has been successfully conducted using a Lattice-Boltzmann method. The important aspect to consider while predicting trailing edge noise lies on the fact that the mesh resolution in the near wall should be fine enough, e.g. such that the surface y^+ is less than 5. As in this work, because of computational cost, this triggered the simulation of an airfoil section with only a short spanwise extension (segmented airfoil) rather an airfoil in a complete wind tunnel. For this case, as compared to experiments, the predicted boundary layer induced surface pressures, near-field velocity fluctuations close to the TE and far field sound pressure are in good agreement. Another important conclusion is that, given a simulation domain of same size, LES requires more computational time and also a finer mesh than a comparable Lattice-Boltzmann method.

ACKNOWLEDGEMENTS

Financial support for this work was partly provided by the Federal Ministry for Economic Affairs and Energy of Germany (BMWi) within the project RENEW (FKZ 0325838B).

The authors would like to thank Franck Perot (Exa Corporation), Marlene Sanjose (University of Sherbrooke) and Tao Zhu (University of Siegen) for their technical assistance in setting up the simulation case as well as Tom Gerhard (Vaillant GmbH) for providing the experimental and LES data.

REFERENCES

- [1] BROOKS, T.F., POPE, D.S., MARCOLINI, M.A., 1989, "Airfoil self-noise and prediction", NASA RP-1218, *NASA Langley Research Center, Hampton, Virginia*.
- [2] OERLEMANS, S., SIJTSMA, P., MÉNDEZ LÓPEZ, B.M., 2007, "Location and quantification of noise sources on a wind turbine", *Journal of Sound and Vibration*, **299**: 869-883.

- [3] GERHARD, T., 2015, "Umströmte Tragflügelsegmente: Auswirkungen des Hinterkantenausblasens auf Strömungsgrenzschicht und Schallemission", *Doctor of Philosophy Thesis*, Universität Siegen.
- [4] GERHARD, T., CAROLUS, T., 2014, "Investigation of airfoil trailing edge noise with advanced experimental and numerical methods", *The 21st International Congress on Sound and Vibration*.
- [5] GERHARD, T., ERBSLÖH, S., CAROLUS, T., 2014, "Reduction of airfoil trailing edge noise by trailing edge blowing", *Journal of Physics*, **524**: 012123.
- [6] CURLE, N., 1955, "The influence of solid boundaries upon aerodynamic sound", *Proceedings of the Royal Society of London. Series A, Mathematical and Physical Sciences*, **231**(1187), pp. 505-514.
- [7] MANN, A., PÉROT, F., KIM, M.S., CASALINO, D., FARES, E., 2012, "Advanced noise control fan direct aeroacoustics predictions using a Lattice-Boltzmann method", *18th AIAA/CEAS Aeroacoustics Conference*.
- [8] ZHU, T., STURM, M., CAROLUS, T., 2014, "Experimental and numerical investigation of tip clearance noise of an axial fan using a Lattice-Boltzmann method", *The 21st International Congress on Sound and Vibration*.
- [9] VAN DER VELDEN, W.C.P., VAN ZUIJLEN, A.H., DE JONG, A.T., BIJL, H., 2015, "On the noise prediction of a serrated DU96 airfoil using the Lattice Boltzmann Method", *6th International Meeting on Wind Turbine Noise*.
- [10] VAN DER VELDEN, W.C.P., VAN ZUIJLEN, A.H., RAGNI, D., 2016, "Flow topology and noise emission around straight, serrated and slitted trailing edges using the Lattice Boltzmann methodology", *22nd AIAA/CEAS Aeroacoustics Conference*.
- [11] SUCCI, S., 2001, "The Lattice Boltzmann Equation for fluid dynamics and beyond", *Oxford University Press*, Oxford.
- [12] BHATNAGAR, P.L., GROSS, E.P., KROOK, M., 1954, "A model for collision processes in gases. I. small amplitude processes in charged and neutral one-component systems", *Physical Review*, **94**(3): 511-525.
- [13] FRISCH, U., HASSLACHER, B., POMEAU, Y., 1986, "Lattice-Gas automata for the Navier-Stokes equation", *Physical Review Letters*, **56**: 1505-1508.
- [14] CHEN, H., CHEN, S., MATTHAEUS, W.H., 1992, "Recovery of the Navier-Stokes equations using a lattice-gas Boltzmann method", *Physical Review A*, **45**(8): R5339-R5342.
- [15] CHEN, S., DOOLEN, G., 1998, "Lattice Boltzmann method for fluid flows", *Annual Review of Fluid Mechanics*, **30**(1): 329-364.
- [16] YAKHOT, V., ORSZAG, S., 1986, "Renormalization group analysis of turbulence. I. basic theory", *Journal of Scientific Computing*, **1**: 3-51.
- [17] CHEN, H., KANDASAMY, S., ORSZAG, S., SHOCK, S., SUCCI, S., YAKHOT, V., 2003, "Extended Boltzmann kinetic equation for turbulent flows", *Science*, **301**: 307-314.
- [18] KOTAPATI, R., SHOCK, R., CHEN, H., 2014, "Lattice-Boltzmann simulations of flows over backward-facing inclined steps", *International Journal of Modern Physics C*, **25**: 1340021.
- [19] BROOKS, T.F., MARCOLINI, M.A., POPE, D.S., 1984, "Airfoil trailing edge flow measurements and comparison with theory incorporating open wind tunnel corrections", *Proc. AIAA/NASA 9th Aeroacoustics Conference*, 1-12.